ACS APPLIED MATERIALS & INTERFACES

Research Article

www.acsami.org

# One-Pot Synthesis of Three-Dimensional Graphene/Carbon Nanotube/$SnO_2$ Hybrid Architectures with Enhanced Lithium Storage Properties

Zheye Zhang, Lu Wang, Jian Xiao, Fei Xiao, and Shuai Wang*

School of Chemistry & Chemical Engineering, Huazhong University of Science and Technology, Wuhan 430074, P. R. China

Supporting Information

**ABSTRACT:** Three-dimensional (3D) graphene/carbon nanotube (CNT)/$SnO_2$ (GCS) hybrid architectures were constructed by a facile and cost-effective self-assembly method through hydrothermal treatment of a mixture of $Sn^{2+}$, CNTs, and graphene oxide (GO). The resultant GCS displayed a 3D hierarchically porous structure with large surface area and excellent electrical conductivity, which could effectively prevent the aggregation and volume variation of $SnO_2$ and accelerate the transport of ions and electrons through 3D pathways. Benefiting from the unique structure and the synergistic effect of different components in the hybrid architectures, the GCS exhibited a remarkably improved reversible capacity of 842 mAh $g^{-1}$ after 100 cycles at 0.2 A $g^{-1}$ and excellent rate performance for lithium storage compared with that of graphene/$SnO_2$ (GS) hybrid architectures. Hence, the impressive results presented here could provide a universal platform for fabricating graphene/CNT-based hybrid architectures with promising applications in various fields.

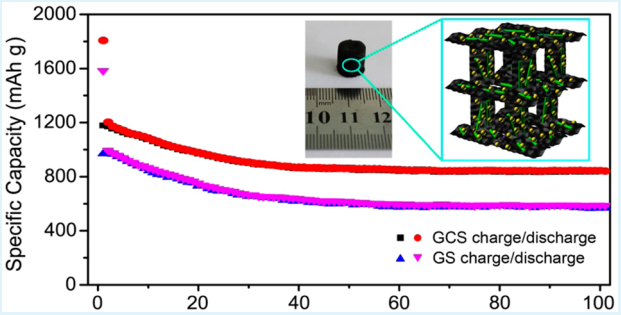


**KEYWORDS:** *one-pot synthesis, $SnO_2$, graphene, carbon nanotubes, hybrid architectures, lithium ion batteries*

## 1. INTRODUCTION

Lithium ion batteries (LIBs) have been intensively utilized in electric vehicles and portable electronics because of their high energy density, relatively low self-discharge, and environmental friendliness.[1−5] To meet the demands for LIBs with higher energy density and excellent cycling performance, much effort has been spent to design both anode and cathode materials with new structures.[6−10] Among various electrode materials, $SnO_2$ is generally considered as a promising anode material candidate because of its high theoretical capacity (780 mAh $g^{-1}$), low toxicity, and widespread availability.[11−13] However, the huge volume changes in $SnO_2$ upon extended Li insertion and/or extraction could give rise to the pulverization and aggregation of electrochemically active particles, which results in low rate capability and poor cycling performance.[14−16] To address these issues, fabricating carbonaceous nanocomposites based on porous carbons,[17−19] carbon nanotubes (CNTs),[20−22] and graphene[23−26] has been demonstrated to be an effective strategy and attracted considerable attention. Although improved electrochemical performances have been achieved, the preparation processes are generally complex, high-cost, and time-consuming, which limit their wide application. Hence, there is an urgent need to develop facile and cost-effective approaches for fabricating high-performance $SnO_2$-based anode composites.

Graphene, with its huge surface area and high conductivity, has been considered as a promising material for energy storage.[27,28] However, the inherent tendency for $\pi-\pi$ stacking interactions of graphene nanosheets greatly reduces their accessible surface area and thereby deteriorates their electrochemical performance. To reduce stacking, graphene/CNT composites, including two-dimensional (2D) hybrid films[29−31] and three-dimensional (3D) hybrid architectures,[32−35] have been proposed and fabricated. The CNTs in the graphene/CNT architectures not only bridge the defects for electron transfer but also efficiently increase the basal spacing between graphene nanosheets.[31] Furthermore, the 3D graphene/CNT architectures exhibit a large specific surface area as well as fast electron and mass transport kinetics because of the combination of porous structures and the excellent intrinsic properties of graphene and CNTs.[34] Therefore, the 3D graphene/CNT architecture would be an ideal substrate to support $SnO_2$ for LIB applications.

Here, we present a facile and cost-effective one-pot hydrothermal self-assembly approach for the fabrication of 3D graphene/CNT/$SnO_2$ (GCS) hybrid architectures, where ultrasmall $SnO_2$ nanoparticles (NPs) were uniformly grown in situ on the 3D graphene/CNT scaffold. Benefiting from the synergistic effects of different components in the hierarchically porous GCS, the resultant hybrid architectures exhibited a

Received: May 28, 2015
Accepted: August 3, 2015
Published: August 3, 2015





DOI: 10.1021/acsami.5b04673
ACS Appl. Mater. Interfaces 2015, 7, 17963−17968

**Scheme 1. Fabrication of GCS Hybrid Architecture**

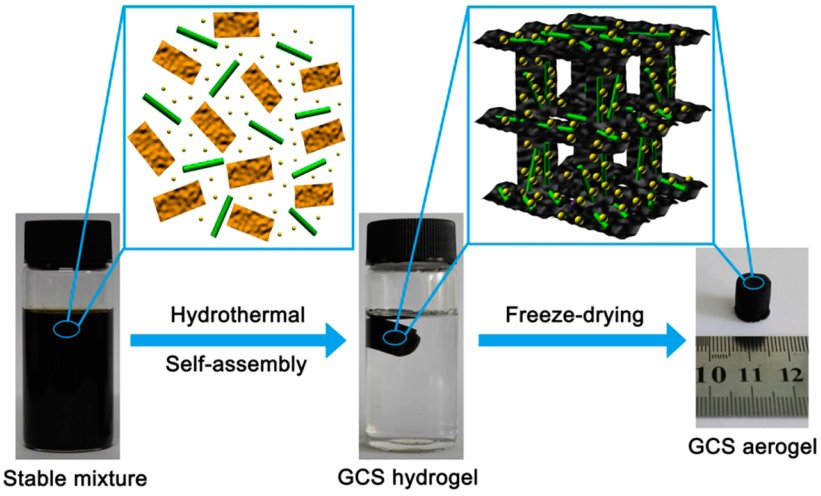


highly reversible capacity of 845 mAh $g^{-1}$ after 100 cycles at 0.2 A $g^{-1}$, with excellent rate capability compared with that of graphene/$SnO_2$ (GS) hybrid architectures, demonstrating a great potential as anode materials in LIBs.

## 2. EXPERIMENTAL SECTION

**2.1. Synthesis of GCS Hybrid Architectures.** GO was prepared through the modified Hummers method;[36] 10 mg of CNTs (>95% pure, from XF NANO, Inc.) were gradually added to the 20 mL GO aqueous dispersion (1 mg $mL^{-1}$). Then, the mixture solution was ultrasonicated for 30 min. Subsequently, 180 mg of tin dichloride dihydrate ($SnCl_2{\cdot}2H_2O$, analytical grade purity, from Sinopharm Chemical Reagent Co. Ltd.) was slowly added to form a stable complex solution while the mixture was stirred for 30 min. Then the suspension was sealed in a 25 mL Teflon-lined autoclave and maintained at 180 °C for 12 h. The 3D GS hybrid architectures were fabricated using a similar procedure without the addition of CNTs.

**2.2. Characterization.** The morphology and structure of samples were characterized with a field-emission scanning electron microscope (GSM6510LV, JEOL) and transmission electron microscope (FEI, Tecnai G2 F30). X-ray photoelectron spectroscopy (XPS) measurements were taken on a VG ESCALAB 250 spectrometer with an Al K$\alpha$ X-ray source (1486 eV), X-ray radiation (15 kV and 10 mA), and hemispherical electron energy analyzer. X-ray powder diffraction (XRD) measurements were performed on a diffractometer (X'Pert PRO, Panalytical B.V.) with a Cu K$\alpha$ radiation source. Thermogravimetic analysis (TGA) was conducted at a heating rate of 10 °C $min^{-1}$ in air. Nitrogen adsorption/desorption isotherms were measured on an accelerated surface area and porosimetry system (ASAP 2020) at 77 K to calculate the surface area of the films by the Brunauer–Emmett–Teller (BET) method.

**2.3. Electrochemical Measurements.** Electrochemical experiments were conducted in 2032 coin cells. To prepare working electrodes, the samples, carbon black (Super-P), and poly(vinyl difluoride) (PVDF) at a weight ratio of 80:10:10 were mixed into a homogeneous slurry and pasted onto pure Cu foil. Pure Li foil was used as the counter electrode. The electrolyte was 1 M $LiPF_6$ in an ethylene carbonate/dimethyl carbonate [EC/DMC, 1:1 (v:v)] mixture. Cell assembly was performed in an argon-filled glovebox. Cyclic voltammetry (CV) was conducted on a CHI 760E electrochemical workstation over a voltage range of 0.005–3.0 V with a scan rate of 0.1 mV $s^{-1}$. The electrochemical impedance spectroscopy (EIS) measurements were also performed on a CHI 760E electrochemical workstation over a frequency range from 100 kHz to 0.1 Hz.

## 3. RESULTS AND DISCUSSION

The synthetic procedure for GCS hybrid architectures is illustrated in Scheme 1. First, the homogeneous GO/CNTs dispersion was obtained by sonication treatment, where the CNTs were well dispersed by an amphiphilic GO solution through $\pi-\pi$ attractions (see Figure S1 of the Supporting Information).[37] Then $SnCl_2{\cdot}2H_2O$ was dissolved in a GO/CNT dispersion to form a stable mixture. During this process, $Sn^{2+}$ was selectively bonded with the oxygenated groups by electrostatic forces.[38] Subsequently, the mixture was hydrothermally assembled at 180 °C for 12 h to form a 3D black hydrogel. In this way, $SnO_2$ NPs could spontaneously nucleate and grow on the surface of graphene and CNTs. This phenomenon can illustrate that the reduction potential of $Sn^{2+}$ is ~0.15 V versus the standard hydrogen electrode (SHE),[39] which is much lower than the oxidation potential of GO (0.72 V vs SHE)[40] or CNT (0.5 V vs SHE).[41] Therefore, the spontaneous oxidation and reduction of GO/$Sn^{2+}$ and CNTs/$Sn^{2+}$ could occur during the hydrothermal assembly process, leading to the formation of desired GCS hybrid architectures.

The morphology of the resultant GCS was characterized by scanning electron microscopy (SEM) and transmission electron microscopy (TEM) (Figure 1). SEM images revealed a well-defined and interconnected 3D porous graphene framework with continuous macropores of micrometer size (Figure 1a,b). Panels c and d of Figure 1 show the TEM images of GCS. It could be seen that ultrasmall $SnO_2$ NPs, with an average size of 4 nm (Figure S2), were uniformly monodispersed on the surfaces of graphene nanosheets and CNTs. However, as for the GS, the $SnO_2$ NPs anchored densely on the graphene nanosheets and almost covered their entire surface (Figure S3), which exhibited serious aggregation for $SnO_2$ NPs in the GS hybrid architectures. The high-resolution TEM (HRTEM) image of GCS (Figure 1e) demonstrates that the crystal lattice fringes of $SnO_2$ NPs were 0.33 and 0.26 nm, which corresponded to the (110) and (101) planes, respectively, of the rutile phase of $SnO_2$. The selected area electron diffraction (SAED) pattern (Figure 1f) further confirmed the presence of both graphene/CNTs (concentric circles) and polycrystalline $SnO_2$ species (broad diffuse rings).

To confirm the chemical compositions of GCS, XPS measurements were performed in the range of 0–800 eV


DOI: 10.1021/acsami.5b04673
ACS Appl. Mater. Interfaces 2015, 7, 17963–17968

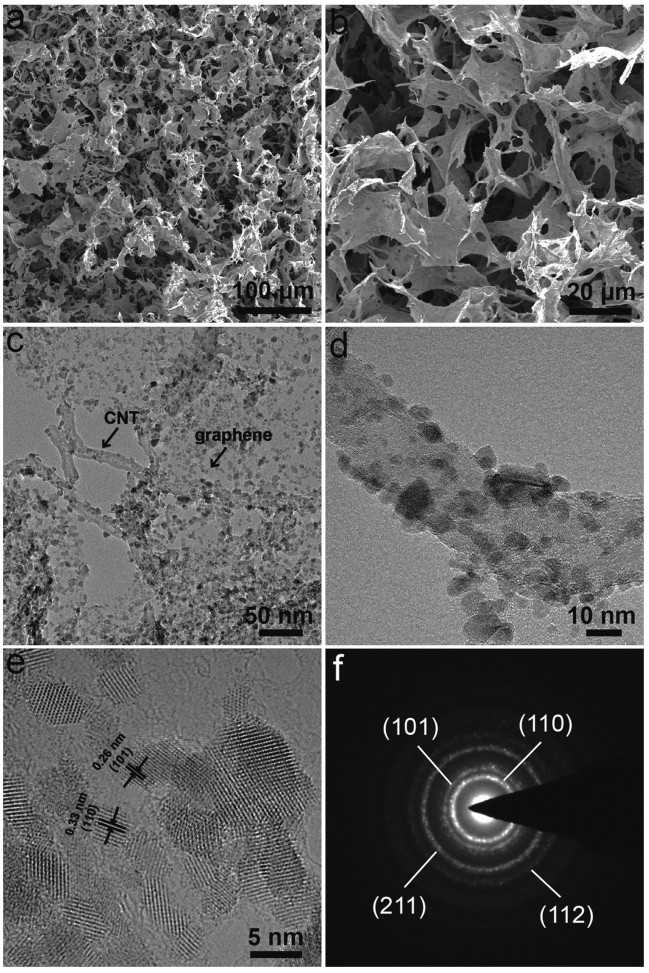


**Figure 1.** (a and b) SEM, (c and d) TEM, and (e) HRTEM images of GCS. (f) Corresponding SAED pattern.

(Figure 2a). The peaks located at the C, O, and Sn core level regions could be assigned to C 1s, O 1s, and Sn 3d, Sn 3p, and Sn 4d, respectively. The deconvoluted C 1s spectrum of GCS (Figure 2b) reveals four types of carbon bonds: C═C/C−C (284.7 eV), C−O (hydroxyl and epoxy, 286.6 eV), C═O (carbonyl, 287.5 eV), and O−C═O (carboxyl, 288.7 eV). In contrast to the C 1s spectrum of GO (Figure S4), the sharp decreases of the signal for oxygen-containing groups in GCS demonstrated a high degree of deoxygenation and successful reduction of GO during the hydrothermal process.[42] Figure 2c shows the high-resolution Sn 3d spectrum. Two peaks centered at 496.4 and 487.9 eV correspond to Sn $3d_{3/2}$ and Sn $3d_{5/2}$, respectively, which was in good agreement with previously reported data for the $SnO_2$ phase.[43]

The obtained GCS and GS were then characterized by XRD (Figure 3a). Both hybrids exhibited similar XRD patterns, in which the major diffraction peaks of $SnO_2$ could be well indentified as a tetragonal rutile-like $SnO_2$ (JCPDS Card No. 41-1445, space group $P4_2/mnm$, $a_0 = b_0 = 4.738$ Å, $c_0 = 3.187$ Å),[44] confirming the HRTEM and SAED observations. However, the (002) diffraction peak for graphene was not observed in the XRD pattern of the GCS, which demonstrated the lack of layer stacking after reduction of GO, because the graphene nanosheets were efficiently assembled into 3D networks and most of the graphene nanosheets were separated by CNTs and $SnO_2$ NPs. TGA of GCS and GS was performed at a heating rate of 10 °C $min^{-1}$ in air to confirm the content by weighting $SnO_2$ in the hybrid architectures. As shown in Figure 3b, the $SnO_2$ contents of GCS and GS were calculated to be ~83.5%. This result indicates that the introduction of CNTs did not influence the component ratio of hybrid materials. The 3D porous structures of GCS and GS were further probed by nitrogen isothermal adsorption/desorption measurements (Figure 3c,d). Obviously, the BET surface area of GCS was 322.5 $m^2$ $g^{-1}$, which was larger than that of GS (234.9 $m^2$ $g^{-1}$). This result highlights that the introduction of CNTs into graphene-based materials was an effective approach to achieving hybrid materials with a large surface area. Furthermore, on the basis of the Barrett−Joyner−Halenda (BJH) model, the pore size of GCS was centered at ~3.7 nm (the inset in Figure 3c). Consequently, the large surface areas of GCS associated with its meso- and macroporous structures are favorable for electrolyte accessibility and rapid $Li^+$ diffusion.

To evaluate the electrochemical performance of the GCS hybrid architectures in LIBs, coin cells with a Li counter electrode were assembled. Figure 4a shows the CV curves for the first two cycles of the GCS electrode at a scan rate of 0.1 mV $s^{-1}$ and cycled between 0.005 and 3 V. The CV behavior is generally consistent with the literature,[45] demonstrating the similar electrochemical process. As observed in the first cycle, the characteristic pair (cathodic and anodic) of current peaks at potentials of 0.27 and 0.61 V should be attributed to the alloying and dealloying of $Li_xSn$ ($0 \le x \le 4.4$) during charge/discharge processes, respectively. Two peaks observed at cathodic and anodic potentials of 1.1 and 1.3 V were ascribed to the reduction and oxidation processes, respectively, suggesting partial reversibility of the reduction of $SnO_2$ to Sn and the synchronous production of $Li_2O$. To probe the advantages of GCS structured architectures with respect to Li storage behavior, the charge/discharge voltage profiles of GCS and GS electrodes at current densities of 0.2 A $g^{-1}$ were

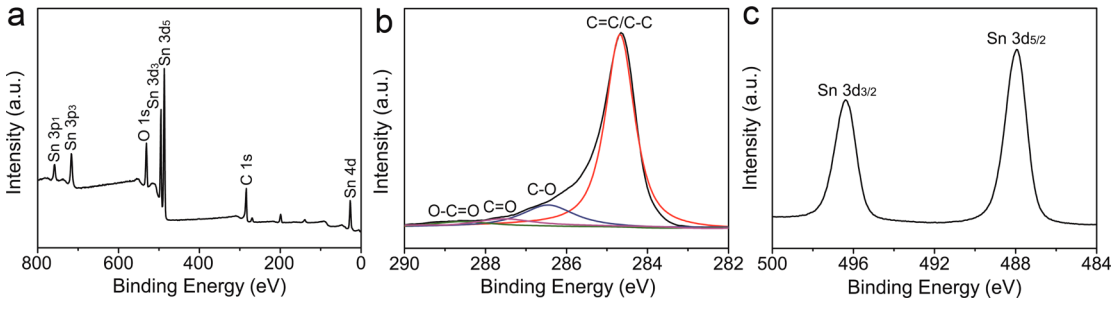


**Figure 2.** (a) XPS survey spectra of GCS. (b) Deconvoluted C 1s spectra of GCS. (c) XPS survey of Sn 3d spectra for GCS.



DOI: 10.1021/acsami.5b04673
ACS Appl. Mater. Interfaces 2015, 7, 17963−17968

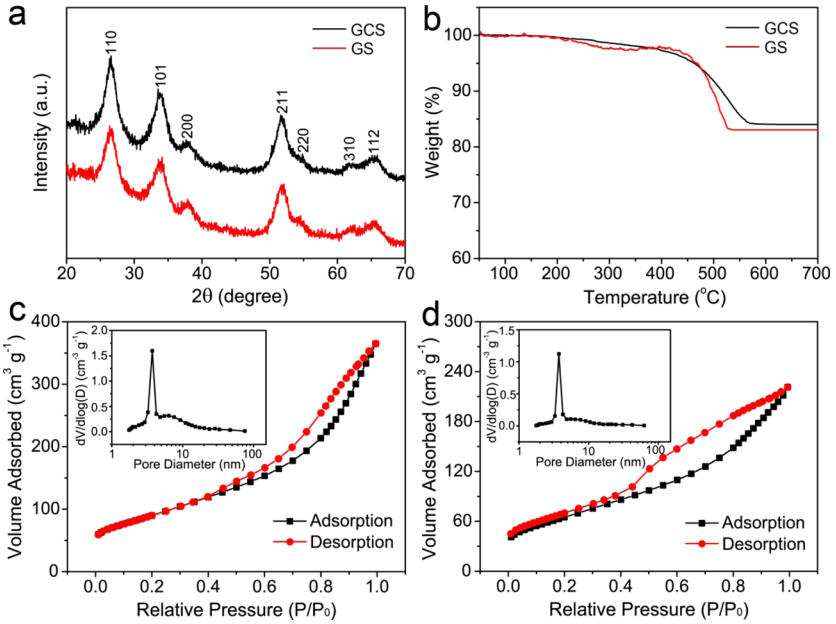


**Figure 3.** (a) XRD patterns and (b) TGA curves of GCS and GS. $N_2$ adsorption−desorption isotherms of (c) GCS and (d) GS. The insets are the corresponding pore size distribution diagrams.

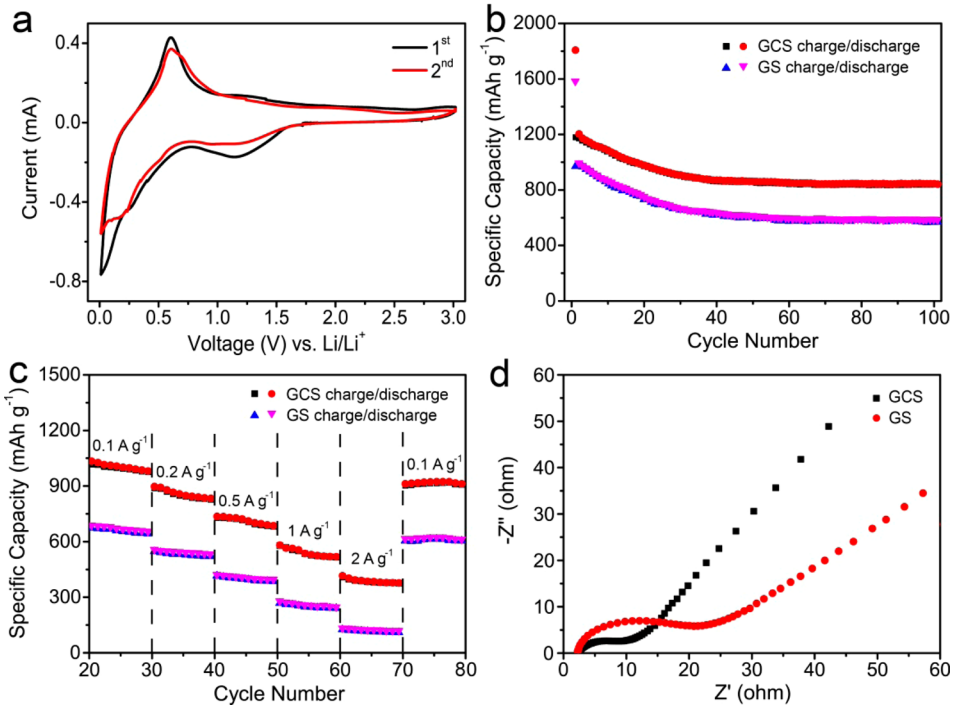


**Figure 4.** (a) CV curves for the first two cycles of the GCS electrode. (b) Cycling performance of GCS and GS electrodes at a current density of 0.2 A $g^{-1}$. (c) Rate performance of GCS and GS electrodes at different current densities. (d) Nyquist plots of GCS and GS electrodes.

measured, as shown in Figure S5. Notably, the GCS electrode delivered a high capacity of approximately 1806 mAh $g^{-1}$ in the first cycle, which was higher than that of the GS electrode (1582 mAh $g^{-1}$), and even the contents of $SnO_2$ were the same in the two electrodes. The capacities of the GCS and GS dropped rapidly after the first cycle because of the irreversible formation of a solid electrolyte interface layer (SEI) and amorphous lithium oxide. Figure 4b shows the cycling performances of GCS and GS electrodes under a current density of 0.2 A $g^{-1}$. The GCS exhibited an excellent reversible capacity of 842 mAh $g^{-1}$ after 40 cycles, which was higher than those of many other reported $SnO_2$-based nanocomposites with different structures.[46−48] However, the GS delievered a stable capacity of only 570 mAh $g^{-1}$ after 50 cycles. The SEM image of GS after cycling (Figure S6a) suggests that $SnO_2$ NPs in GS exhibited obvious pulverization and aggregation after 100 cycles. In contrast, the primary dispersibility of $SnO_2$ NPs in GCS was preserved, demonstrating a good restraint for the aggregation of $SnO_2$ upon cycling (Figure S6b).


DOI: 10.1021/acsami.5b04673
ACS Appl. Mater. Interfaces 2015, 7, 17963−17968

The rate capability is also vital for evaluating the electrochemical performance of LIBs. Figure 4c demonstrates the rate performance of GCS and GS at different current densities (0.1, 0.2, 0.5, 1, and 2 A $g^{-1}$). As the current density increased from 0.1 to 2 A $g^{-1}$, the GCS electrode preserved 40% of its initial capacity (from 1040 to 414 mAh $g^{-1}$). In comparison, the reversible capacity of the GS electrode decreased quickly from 688 to 124 mAh $g^{-1}$; only 18% of the initial capacity was maintained. When the current density was returned to 0.1 A $g^{-1}$, the stable high capacity of GCS (923 mAh $g^{-1}$, 89% of the initial capacity) was retained. To further demonstrate the superior electrochemical performance of GSC compared with that of the GS electrode, AC impedance tests were performed. The Nyquist plots (Figure 4d) show that the diameter of the semicircle for GCS was much smaller than that of GS, suggesting lower contact and charge-transfer resistances of GCS compared with those of GS. The kinetic differences of the GCS and GS electrodes were further surveyed by a simulated Randles equivalent circuit (Figure S7 and Table S1). The values for the surface film resistance ($R_f$) and the charge-transfer resistance ($R_{ct}$) for the GCS electrode were 2.1 and 4.8 Ω, respectively, which were lower than those for the GS electrode (4.3 and 13.5 Ω, respectively). On the basis of the results described above, the introduction of CNTs not only greatly improved the electrochemical activity of the hybrid architecture but also enhanced the electrical conductivity of the electrode.

The enhanced electrochemical performance of GCS as an anode material for Li storage can be attributed to the following factors. First, the construction of the 3D hierarchically porous graphene/CNT architecture creates a large surface area for the in situ growth of the ultrasmall $SnO_2$ NPs in the structure, preventing the serious aggregation of the $SnO_2$ NPs on the bare graphene nanosheets. Second, the elastic graphene/CNT networks that act as a buffer could accommodate the volume changes of $SnO_2$ NPs during the charge/discharge process. Third, the 3D conductive frameworks with macro- and mesoporous features and a large surface area could provide efficient pathways to facilitate the transport of electrons, improve the adsorption of $Li^+$, and shorten the diffusion paths for rapid $Li^+$ insertion and extraction in the bulk electrode.

## 4. CONCLUSION

In summary, a facile and cost-effective strategy has been successfully developed for the fabrication of GCS hybrid architectures with a 3D hierarchically porous conducting network structure through the hydrothermal treatment of a mixture of $Sn^{2+}$, CNTs, and GO. Such a unique architecture established by graphene nanosheets and CNTs exhibited a meso- and macroporous structure with a large surface area and excellent electrical conductivity, which could work effectively against the volume changes and aggregation of $SnO_2$ and ensures favorable transport kinetics for both $Li^+$ and electrons. As a result, the GCS displays a remarkably enhanced capacity of 842 mAh $g^{-1}$ at 0.2 A $g^{-1}$ after 40 cycles, as well as excellent rate performance compared with that of GS, indicating a great potential as an anode material in LIBs. We believe the proposed facile synthesis route will be a universal platform for fabricating graphene/CNT-based hybrid architectures that can be used in a wide range of sensing, catalysis, supercapacitors, and fuel cells.

## ■ ASSOCIATED CONTENT

### Supporting Information

The Supporting Information is available free of charge on the ACS Publications website at DOI: 10.1021/acsami.5b04673.

TEM images, XPS data, charge/discharge profiles, and a particle size distribution histogram (PDF)

## ■ AUTHOR INFORMATION

### Corresponding Author

*E-mail: chmsamuel@mail.hust.edu.cn.

### Notes

The authors declare no competing financial interest.

## ■ ACKNOWLEDGMENTS

This research was financially supported by the National Natural Science Foundation of China (Projects 51173055 and 21305048) and the National Program on Key Basic Research Project (973 Program, Grant 2013CBA01600).

## ■ REFERENCES

(1) Kang, K.; Meng, Y. S.; Bréger, J.; Grey, C. P.; Ceder, G. Electrodes with High Power and High Capacity for Rechargeable Lithium Batteries. *Science* **2006**, *311*, 977−980.
(2) Chan, C. K.; Peng, H.; Liu, G.; McIlwrath, K.; Zhang, X. F.; Huggins, R. A.; Cui, Y. High-Performance Lithium Battery Anodes Using Silicon Nanowires. *Nat. Nanotechnol.* **2008**, *3*, 31−35.
(3) Kang, B.; Ceder, G. Battery Materials for Ultrafast Charging and Discharging. *Nature* **2009**, *458*, 190−193.
(4) Armand, M.; Grugeon, S.; Vezin, H.; Laruelle, S.; Ribière, P.; Poizot, P.; Tarascon, J. M. Conjugated Dicarboxylate Anodes for Li-Ion Batteries. *Nat. Mater.* **2009**, *8*, 120−125.
(5) Recham, N.; Chotard, J. N.; Dupont, L.; Delacourt, C.; Walker, W.; Armand, M.; Tarascon, J. M. A 3.6 V Lithium-Based Fluorosulphate Insertion Positive Electrode for Lithium-Ion Batteries. *Nat. Mater.* **2010**, *9*, 68−74.
(6) Armand, M.; Tarascon, J. M. Building Better Batteries. *Nature* **2008**, *451*, 652−657.
(7) Goodenough, J. B.; Kim, Y. Challenges for Rechargeable Li Batteries. *Chem. Mater.* **2010**, *22*, 587−603.
(8) Jiang, J.; Li, Y.; Liu, J.; Huang, X.; Yuan, C.; Lou, X. W. D. Recent Advances in Metal Oxide-based Electrode Architecture Design for Electrochemical Energy Storage. *Adv. Mater.* **2012**, *24*, 5166−5180.
(9) Janoschka, T.; Hager, M. D.; Schubert, U. S. Powering Up the Future: Radical Polymers for Battery Applications. *Adv. Mater.* **2012**, *24*, 6397−6409.
(10) Chen, J. S.; Lou, X. W. D. $SnO_2$-Based Nanomaterials: Synthesis and Application in Lithium-Ion Batteries. *Small* **2013**, *9*, 1877−1893.
(11) Idota, Y.; Kubota, T.; Matsufuji, A.; Maekawa, Y.; Miyasaka, T. Tin-Based Amorphous Oxide: A High-Capacity Lithium-Ion-Storage Material. *Science* **1997**, *276*, 1395−1397.
(12) Wang, C.; Zhou, Y.; Ge, M.; Xu, X.; Zhang, Z.; Jiang, J. Z. Large-Scale Synthesis of $SnO_2$ Nanosheets with High Lithium Storage Capacity. *J. Am. Chem. Soc.* **2010**, *132*, 46−47.
(13) Zhang, L.; Zhang, G.; Wu, H. B.; Yu, L.; Lou, X. W. D. Hierarchical Tubular Structures Constructed by Carbon-Coated $SnO_2$ Nanoplates for Highly Reversible Lithium Storage. *Adv. Mater.* **2013**, *25*, 2589−2593.
(14) Larcher, D.; Beattie, S.; Morcrette, M.; Edström, K.; Jumas, J. C.; Tarascon, J. M. Recent Findings and Prospects in the Field of Pure Metals as Negative Electrodes for Li-Ion Batteries. *J. Mater. Chem.* **2007**, *17*, 3759−3772.
(15) Chen, Z.; Zhou, M.; Cao, Y.; Ai, X.; Yang, H.; Liu, J. In Situ Generation of Few-Layer Graphene Coatings on $SnO_2$-SiC Core-Shell Nanoparticles for High-Performance Lithium-Ion Storage. *Adv. Energy Mater.* **2012**, *2*, 95−102.


DOI: 10.1021/acsami.5b04673
ACS Appl. Mater. Interfaces 2015, 7, 17963−17968

(16) Han, F.; Li, W. C.; Li, M. R.; Lu, A. H. Fabrication of Superior-Performance $SnO_2$@C Composites for Lithium-Ion Anodes Using Tubular Mesoporous Carbon with Thin Carbon Walls and High Pore Volume. *J. Mater. Chem.* **2012**, *22*, 9645−9651.
(17) Lou, X. W.; Li, C. M.; Archer, L. A. Designed Synthesis of Coaxial $SnO_2$@ Carbon Hollow Nanospheres for Highly Reversible Lithium Storage. *Adv. Mater.* **2009**, *21*, 2536−2539.
(18) Liang, J.; Yu, X. Y.; Zhou, H.; Wu, H. B.; Ding, S.; Lou, X. W. D. Bowl-Like $SnO_2$@Carbon Hollow Particles as an Advanced Anode Material for Lithium-Ion Batteries. *Angew. Chem., Int. Ed.* **2014**, *53*, 12803−12807.
(19) Ko, Y. N.; Park, S. B.; Kang, Y. C. Design and Fabrication of New Nanostructured $SnO_2$-Carbon Composite Microspheres for Fast and Stable Lithium Storage Performance. *Small* **2014**, *10*, 3240−3245.
(20) Guo, Z. P.; Zhao, Z. W.; Liu, H. K.; Dou, S. X. Electrochemical Lithiation and Delithiation of MWNT-Sn/SnNi Nanocomposites. *Carbon* **2005**, *43*, 1392−1399.
(21) Zhang, B.; Zheng, Q. B.; Huang, Z. D.; Oh, S. W.; Kim, J. K. $SnO_2$-Graphene-Carbon Nanotube Mixture for Anode Material with Improved Rate Capacities. *Carbon* **2011**, *49*, 4524−4534.
(22) Hu, R.; Sun, W.; Liu, H.; Zeng, M.; Zhu, M. The Fast Filling of Nano-$SnO_2$ in CNTs by Vacuum Absorption: A New Approach to Realize Cyclic Durable Anodes for Lithium Ion Batteries. *Nanoscale* **2013**, *5*, 11971−11979.
(23) Luo, B.; Wang, B.; Li, X.; Jia, Y.; Liang, M.; Zhi, L. Graphene-Confined Sn Nanosheets with Enhanced Lithium Storage Capability. *Adv. Mater.* **2012**, *24*, 3538−3543.
(24) Zhou, X.; Wan, L. J.; Guo, Y. G. Binding $SnO_2$ Nanocrystals in Nitrogen-Doped Graphene Sheets as Anode Materials for Lithium-Ion Batteries. *Adv. Mater.* **2013**, *25*, 2152−2157.
(25) Ye, F.; Zhao, B.; Ran, R.; Shao, Z. Facile Mechanochemical Synthesis of Nano $SnO_2$/Graphene Composite from Coarse Metallic Sn and Graphite Oxide: An Outstanding Anode Material for Lithium-Ion Batteries. *Chem. - Eur. J.* **2014**, *20*, 4055−4063.
(26) Pei, L.; Jin, Q.; Zhu, Z.; Zhao, Q.; Liang, J.; Chen, J. Ice-Templated Preparation and Sodium Storage of Ultrasmall $SnO_2$ Nanoparticles Embedded in Three-Dimensional Graphene. *Nano Res.* **2015**, *8*, 184−192.
(27) Huang, X.; Zeng, Z.; Fan, Z.; Liu, J.; Zhang, H. Graphene-Based Electrodes. *Adv. Mater.* **2012**, *24*, 5979−6004.
(28) Simon, P.; Gogotsi, Y. Capacitive Energy Storage in Nanostructured Carbon-Electrolyte Systems. *Acc. Chem. Res.* **2013**, *46*, 1094−1103.
(29) Fan, Z.; Yan, J.; Zhi, L.; Zhang, Q.; Wei, T.; Feng, J.; Wei, F. A Three-Dimensional Carbon Nanotube/Graphene Sandwich and Its Application as Electrode in Supercapacitors. *Adv. Mater.* **2010**, *22*, 3723−3728.
(30) Yu, D.; Dai, L. Self-Assembled Graphene/Carbon Nanotube Hybrid Films for Supercapacitors. *J. Phys. Chem. Lett.* **2010**, *1*, 467−470.
(31) Yuan, C.; Yang, L.; Hou, L.; Li, J.; Sun, Y.; Zhang, X.; Lou, X. W. D. Flexible Hybrid Paper Made of Monolayer $Co_3O_4$ Microsphere Arrays on rGO/CNTs and Their Application in Electrochemical Capacitors. *Adv. Funct. Mater.* **2012**, *22*, 2560−2566.
(32) Sun, T.; Zhang, Z.; Xiao, J.; Chen, C.; Xiao, F.; Wang, S.; Liu, Y. Facile and Green Synthesis of Palladium Nanoparticles-Graphene-Carbon Nanotube Material with High Catalytic Activity. *Sci. Rep.* **2013**, *3*, 2527.
(33) Sun, H.; Xu, Z.; Gao, C. Multifunctional, Ultra-Flyweight, Synergistically Assembled Carbon Aerogels. *Adv. Mater.* **2013**, *25*, 2554−2560.
(34) Zhang, Z.; Sun, T.; Chen, C.; Xiao, F.; Gong, Z.; Wang, S. Bifunctional Nanocatalyst Based on Three-Dimensional Carbon Nanotube-Graphene Hydrogel Supported Pd Nanoparticles: One-Pot Synthesis and Its Catalytic Properties. *ACS Appl. Mater. Interfaces* **2014**, *6*, 21035−21040.
(35) Yu, D.; Goh, K.; Wang, H.; Wei, L.; Jiang, W.; Zhang, Q.; Chen, Y. Scalable Synthesis of Hierarchically Structured Carbon Nanotube-Graphene Fibres for Capacitive Energy Storage. *Nat. Nanotechnol.* **2014**, *9*, 555−562.
(36) Hummers, W. S.; Offeman, R. E. Preparation of Graphitic Oxide. *J. Am. Chem. Soc.* **1958**, *80*, 1339.
(37) Kim, J.; Cote, L. J.; Kim, F.; Yuan, W.; Shull, K. R.; Huang, J. Graphene Oxide Sheets at Interfaces. *J. Am. Chem. Soc.* **2010**, *132*, 8180−8186.
(38) Zhong, L. S.; Hu, J. S.; Cui, Z. M.; Wan, L. J.; Song, W. G. In-Situ Loading of Noble Metal Nanoparticles on Hydroxyl-Group-Rich Titania Precursor and Their Catalytic Applications. *Chem. Mater.* **2007**, *19*, 4557−4562.
(39) Bard, A. J.; Parsons, R.; Jordan, J. *Standard potentials in aqueous solution*; Marcel Dekker: New York, 1985.
(40) Chen, X.; Wu, G.; Chen, J.; Chen, X.; Xie, Z.; Wang, X. Synthesis of "Clean" and Well-Dispersive Pd Nanoparticles with Excellent Electrocatalytic Property on Graphene Oxide. *J. Am. Chem. Soc.* **2011**, *133*, 3693−3695.
(41) Qu, L. T.; Dai, L. Substrate-Enhanced Electroless Deposition of Metal Nanoparticles on Carbon Nanotubes. *J. Am. Chem. Soc.* **2005**, *127*, 10806−10807.
(42) Xu, Y.; Sheng, K.; Li, C.; Shi, G. Self-Assembled Graphene Hydrogel via a One-Step Hydrothermal Process. *ACS Nano* **2010**, *4*, 4324−4330.
(43) Lin, Y. S.; Duh, J. G.; Hung, M. H. Shell-by-Shell Synthesis and Applications of Carbon-Coated $SnO_2$ Hollow Nanospheres in Lithium-Ion Battery. *J. Phys. Chem. C* **2010**, *114*, 13136−13141.
(44) Wang, C.; Zhou, Y.; Ge, M.; Xu, X.; Zhang, Z.; Jiang, J. Z. Large-Scale Synthesis of $SnO_2$ Nanosheets with High Lithium Storage Capacity. *J. Am. Chem. Soc.* **2010**, *132*, 46−47.
(45) Wu, P.; Du, N.; Zhang, H.; Zhai, C.; Yang, D. Self-Templating Synthesis of $SnO_2$-Carbon Hybrid Hollow Spheres for Superior Reversible Lithium Ion Storage. *ACS Appl. Mater. Interfaces* **2011**, *3*, 1946−1952.
(46) Xu, C.; Sun, J.; Gao, L. Controllable Synthesis of Monodisperse Ultrathin $SnO_2$ Nanorods on Nitrogen-Doped Graphene and Its Ultrahigh Lithium Storage Properties. *Nanoscale* **2012**, *4*, 5425−5430.
(47) Wang, L.; Wang, D.; Dong, Z.; Zhang, F.; Jin, J. Interface Chemistry Engineering for Stable Cycling of Reduced GO/$SnO_2$ Nanocomposites for Lithium Ion Battery. *Nano Lett.* **2013**, *13*, 1711−1716.
(48) Vinayan, B. P.; Ramaprabhu, S. Facile Synthesis of $SnO_2$ Nanoparticles Dispersed Nitrogen Doped Graphene Anode Material for Ultrahigh Capacity Lithium Ion Battery Applications. *J. Mater. Chem. A* **2013**, *1*, 3865−3871.


DOI: 10.1021/acsami.5b04673
*ACS Appl. Mater. Interfaces* 2015, 7, 17963−17968